Journal of Marine Research, 54, 589–603, 1996

A high resolution camera system (ParCa) for imaging particles in the ocean: System design and results from profiles and a three-month deployment

by Volker Ratmeyer[1] and Gerold Wefer[1]

ABSTRACT

For direct optical measurement of abundance, concentration and size distribution of marine particles, a high-resolution camera system (ParCa) was designed to improve on similar systems used by Honjo *et al.* (1984), Asper (1987) and others. Imaging a probe volume of up to 37 l, smallest particles with diameters of 50 μm can be counted. The images provide information on particle size, shape and abundance either during profiling through the water column or while moored in a certain depth over time. Depth profiles were acquired between fall 1992 and late spring 1993 on R. V. *Meteor* cruises M22-1 and M23-3 at 6 stations in the equatorial Atlantic Ocean and off the west African shelf. The images show variable particle and aggregate concentrations through 550 m of the water column, with highest concentrations in the upper 80 m. A distinctive change in the depth of the upper chlorophyll maximum from about 75 m in the Brazil Basin to about 50 m in the Guinea Basin was measured with the attached INFLUX current meter (Krause and Ohm, 1996) and is as well represented in the particle abundances of two selected profiles. In contrast, both profiles show a second particle abundance maximum between 100 and 250 m, which is not visible in the chlorophyll-*a* and backscatter signal of the INFLUX sensors. Total particle abundance maxima raise from 677 counts per liter in the central Brazil Basin to 991 counts in the Guinea Basin, corresponding to marine snow abundances of 57 and 127 counts per liter, respectively.

In order to compare high-resolution data on particle concentration and flux through time, ParCa was also deployed on a sediment-trap mooring at 995 m depth in the Canary Basin between June and September 1994. First results show similar trends in sediment-trap derived fluxes of particulate matter from 2.8 to 67.2 mg m^{-2} d^{-1} and equivalent spherical volumes of particles with diameters >0.5 mm from 0.98 to 4.13 mm^3 l^{-1}.

1. Introduction

Most marine particles and aggregates are produced in the upper few hundred meters of the ocean, and they are known to be the most important carbon and element carriers from the ocean's surface to the deep sea. Recent investigations of particle fluxes throughout the world's oceans (Honjo *et al.,* 1982; Deuser, 1986; Wefer, 1989; Fischer *et al.,* 1996) show the necessity to obtain detailed knowledge about the various origins, transportation, alteration processes and pathways of

1. Fachbereich Geowissenschaften, Universität Bremen, Klagenfurter Str., 28359 Bremen, Germany.

particles through the water column. Most of the common hydrocasting and flux-recording methods allow the record of composition, seasonality patterns and flux through time, but significantly less data are available concerning *in-situ* size, settling behavior and high-frequency changes in the abundance of particles and aggregates through the water column (Lampitt *et al.,* 1993; Syvitski *et al.,* 1995; MacIntire *et al.,* 1995).

Although it has been proposed that particle flux and sedimentation in the deep ocean is mainly driven by large, rapidly-sinking aggregates in the size class of marine snow (defined as aggregated particles of a diameter greater than 0.5 mm) (McCave, 1975), evidence in the form of *in-situ* observation of abundance and sinking speed of particles in all size classes is based only on a small number of observations. This is mainly due to the extremely delicate nature of marine aggregates which are generally not preserved in trapped material. Except for the fast sinking and stable fecal pellets, most forms of marine aggregates are very fragile and thus require the use of nondestructive methods for observation and very advanced sampling techniques. Successful approaches include the use of submersibles (Kajihara, 1971; Silver and Alldredge, 1981), SCUBA techniques (Shanks and Trent, 1980), various photographic systems and video observation techniques (Honjo *et al.,* 1984; Lampitt, 1985; Asper, 1987; Hecker, 1990; Heffler *et al.,* 1991; Asper *et al.,* 1992; Gorsky *et al.,* 1992; Lampitt *et al.,* 1993; MacIntire *et al.,* 1995; Syvitski *et al.,* 1995), holographic imaging techniques (Costello *et al.,* 1989) and the use of transmissometers and fluorometers (Gardner and Richardson, 1992; Krause and Ohm, 1995), or combinations of those. Although each technique has its clear advantages, only a few can be used to observe a broad spectrum of particle sizes, their sinking speed and composition *in situ* especially over long time periods and at great water depths.

The particle camera system (ParCa) presented in this paper improves on the photographic method developed by Honjo *et al.* (1984) and provides *in-situ* information on the abundance, concentration and size spectra of marine particles and aggregates while using the highest resolving optics and film format available for underwater observations. ParCa was used between fall 1992 and late spring 1993 at several stations in the equatorial Atlantic Ocean and off the west African shelf for particle size and abundance measurements through the upper 550 m of the water column. During these cruises the system was used to a water depth of 600 m. Between June and September 1994, ParCa was deployed in a sediment-trap mooring at 995 m depth in the Canary Basin.

In this paper, we describe the technical setup of the ParCa system and show the first results on particle size, abundance and estimated spherical volumes obtained during the first deployments in different areas of the Atlantic Ocean. A detailed discussion of these data in comparison to particle sinking speeds and fluxes measured with sediment traps will be presented and discussed elsewhere.

2. Methods

Improving on similar photographic devices used by Honjo *et al.* (1984), Lampitt (1985) and Asper (1987) the system presented here combines the advantage of high resolution photographic observation techniques with the needs of illuminating large probe volumes to image a broad spectrum of particle sizes, ranging from 0.05 mm to 0.4 m. It provides a sampling capacity of up to 650 images, which allows a high sampling frequency during moored deployments and gives a high spatial resolution of the particle distribution when lowered through the water column. To augment the use of sediment traps, particle concentration can be measured even in areas or depths with high lateral transport.

To obtain oceanographic data and additional optical measurements during profiling, an INFLUX current meter with CTD-sensors, fluorometer and backscattering sensor (Krause and Ohm, 1996) was mounted to the system. Both optical sensors had the same source of excitation (flashlight, broad band up to 520 nm), the detection range was 680 ± 10 nm for fluorescence and broad band for backscattering. Sampling volume was 1 ml for the fluorescence and 20 l for the backscattering sensor. Additional instrument specifications are given in Krause and Ohm (1996).

ParCa can be operated remote-controlled when lowered through the water column or autonomous when attached to a mooring during long-time deployment. Maximum operating depth is 6000 m.

a. System setup. To get the highest possible optical resolution in the images, ParCa consists of a submersible photographic camera system (Fig. 1a) instead of a video setup. Both camera (PHOTOSEA 70) and strobe lights (PHOTOSEA 1500SD) are commercially available, though camera and strobe electronics had to be modified for long-time deployment. The main advantage of the camera is the 6 × 6 cm negative-format which provides about four times higher resolution than similar systems based on 35 mm film or highest-resolution video. The camera can hold up to 650 frames using thin-based film.

The best optical setup of camera and light source for *in-situ* imaging of highly hydrated particles and aggregates was described by Honjo *et al.* (1984). To calculate particle abundance and concentrations, it is necessary to know the volume of water represented in the images. Thus, the light source at the focal distance of 60 cm is fixed orthogonal to the optical axis of the camera (Fig. 1b). It consists of two sets of highly refractive acrylic fresnel lenses—the collimator—in front of the two strobe lights. This setup produces a collimated light beam covering the area of 60 × F cm, where F is the thickness of the light beam, given by the collimator's aperture and the depth of field of the viewing optics. Typical aperture setting was f-stop 11, resulting in F = 12 cm depth of field and a 12 cm wide light slab, which was verified using a metric calibration setup and a test tank. The viewed probe volume due to the lens viewing angle of 50° was then 44 × 44 × 12 cm, or 24 l. Maximum depth of field was F =

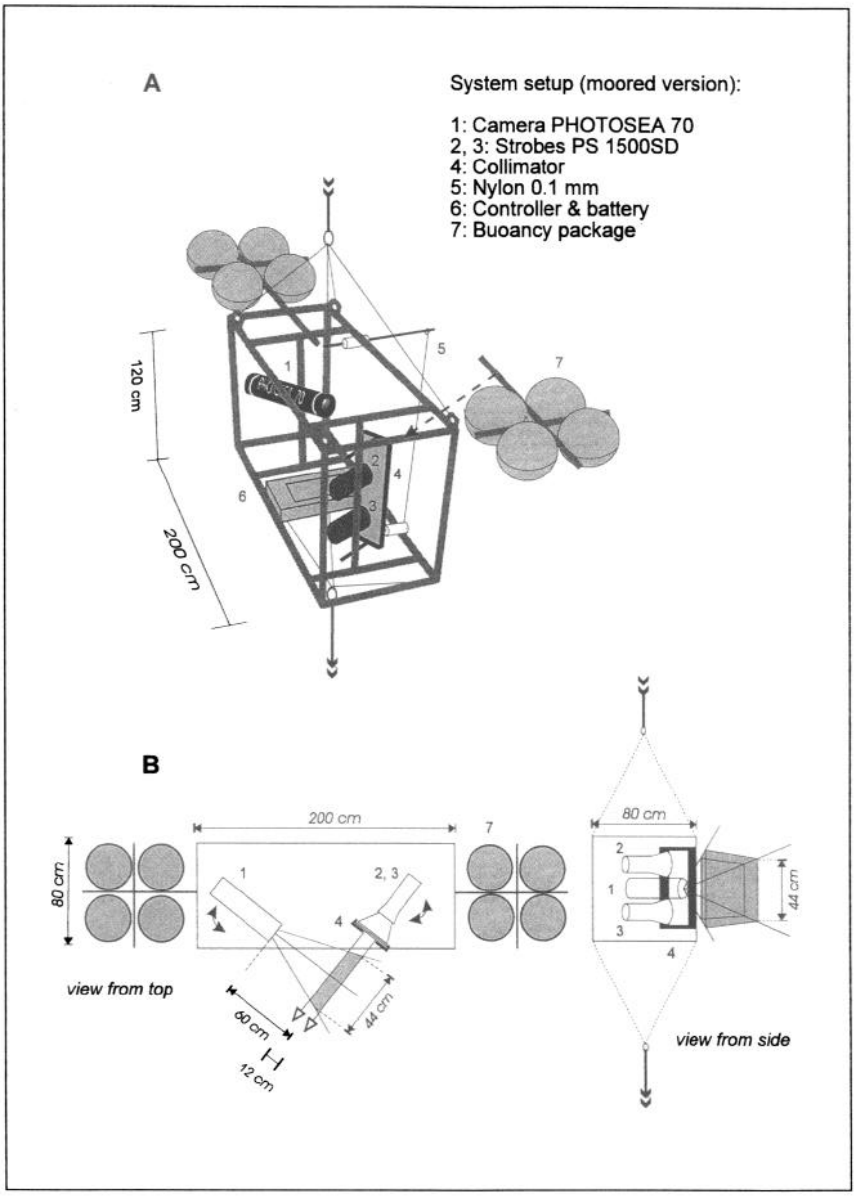

Figure 1. Schematic view (A) and optical setup (B) of the ParCa system used in this study.

19 cm using f-stop 16, providing 37 l maximum probe volume. Maximum *in-situ* resolution is 0.05 mm, using KODAK Technical Pan film, and around 0.08 mm using KODAK Tri X Pan Film. The Tri X Pan allows forced film processing at 800 to 1600 ASA and can therefore be used with higher f-stop settings due to greater depth of field and larger probe volumes.

The power-supply, camera and flashlights are controlled by a PIC-processor based microcomputer which is installed in a separate pressure housing. Both software and the electronic interface between controller, camera and external PC were developed at the Marine Geology Group at the University of Bremen. During vertical profiling, exposure is triggered either by the controller-unit or via cable by a PC on deck of the research vessel. For long-time and moored deployment, a set of control options can be programmed: start-time of exposure program, time interval between single frames, time interval between multi-exposures on a single frame, multi-exposure/single exposure rate, total number of frames to be exposed and number of test runs when power is switched on. Because a major limitation of the system is given by the camera's film-capacity, any combination of single and multiple exposures may be set. Using the multi-exposure option with interval times greater than the assumed slowest sinking time of particles through the camera's field of view, the final image gives the particle distribution inside a water volume as large as n-times the illuminated volume, where n is the number of exposures in one single frame. This approach is only used during moored deployment.

Frame number and number of exposures per frame are recorded on each image by a second PIC-processor and LED's inside the camera. Power is supplied by a pressure resistant, nonliquid, rechargeable 24V/38Ah lead acid battery (manufactured by DeepSea Power & Light). All components of the ParCa system are installed inside a hot-galvanized steel frame, whose dimensions are 2 m × 1.2 m × 0.8 m (Fig. 1a). Total weight in air is 310 kg, weight in water is approximately 250 kg. While the system is attached to a mooring, two buoyancy packages each holding 4 glass spheres are mounted to the frame.

b. Image digitizing and analysis. Quantitative analysis of particle abundance and size is performed by digital image analysis. The image analysis setup consists of a modified photographic enlarger, a Sony single-chip CCD color camera, a Sony Trinitron monitor for image control and an IBM compatible Pentium personal computer with 17″ color display. Images are captured using an 8 bit grayscale video framegrabber (MuTech Image VGA plus) inside the computer, allowing a resolution of 768 × 512 pixels. A menu-driven software package (BioScan Optimas) is used for capturing, processing and analysis of the images. Its powerful C-library of image-analysis related algorithms and functions was used to create complex macros for image enhancement and process automatization. A flowchart showing the procedure of data acquisition, image-analysis and data processing is given in Figure 2. Images showing zooplankton were excluded from measurements.

c. Image capturing. A variable tube extends the optical pathlength between negative and lens of the enlarger and reduces negative size to the ½ inch diameter of the camera's CCD chip. This allows the entire image to be digitized but provides only

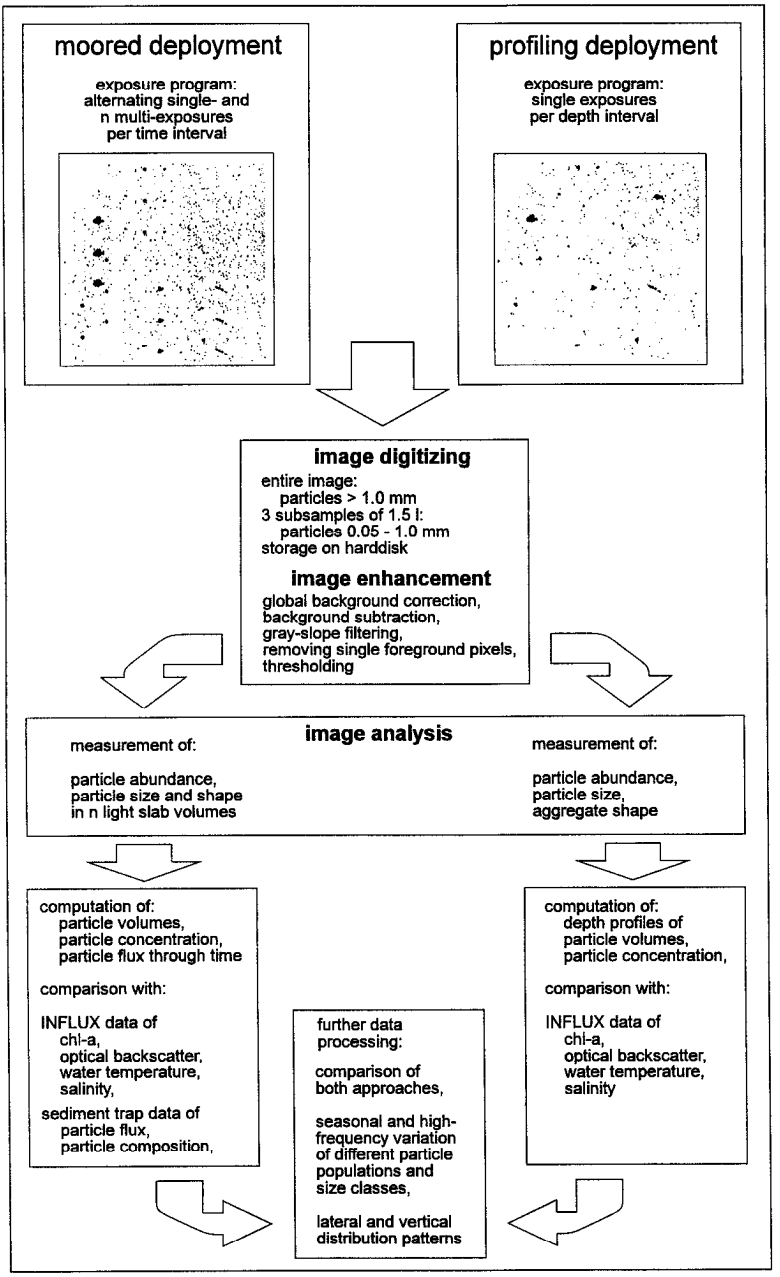

Figure 2. Flowchart showing the procedure of image acquisition, image-analysis and data processing used at the Marine Geology Group at the University of Bremen.

low optical resolution. Because the optical resolution of the digitizing system is limited by hardware to 768 × 512 pixels, different magnifications have to be set for measuring different size classes of particles in the original image. A transparent overlay is used to define subsamples in the photographic frame. This method allows the detection of rare particles in the size class of marine snow as well as the use of the high resolution to record smallest particles with diameters of 0.5 mm.

d. Image processing. Even though illumination in the ParCa system is collimated, slight gray-shading of the background and sometimes illumination of particles out of focus is not avoidable. Thus, each image is enhanced digitally to provide the best accuracy for measuring particle size and concentration. This is done by automated background correction, background subtraction, removing single foreground pixels and thresholding foreground pixels. Particles out of focus can clearly be recognized and are removed using a gray-slope filter, which identifies unsharp particles from the gradient of background to thresholded foreground gray values. For all images exposed on the same profile, edge-values for background correction and thresholding are not changed due to equal illumination during deployment time. Every step of image enhancement can be controlled by overlaying the thresholded foreground, the enhanced image and the originally grabbed frame.

e. Image analysis. Particles are identified automatically after image enhancement is performed. Data of particle area, major and minor axis length are directly exported into a Microsoft Excel worksheet. All particles are assumed to lie along the mid-plane of the illuminated probe volume. Equivalent spherical diameter and volume are calculated for each individual particle, assuming spherical shape. Seven size classes (<0.1 mm (A), 0.1–0.25 mm (B), 0.25–0.5 mm (C), 0.5–0.75 mm (D), 0.75–1.0 mm (E), 1.0–2.0 mm (F) and >2.0 mm (G)) are defined to characterize the size distribution. Particles >1.0 mm diameter are recorded using the entire photographic frame, whereas the smaller size classes are measured using subsamples of the image representing an *in-situ* volume of 1.5 liters.

f. Sediment-trap samples. During moored deployment, samples were collected with cone-shaped sediment traps with 0.5 m^2 openings (Aquatec, Kiel, FRG) at 923 and 3070 m water depth. Sample cups were poisoned with mercuric chloride prior to and after recovery. The collected material was treated as described in Fischer and Wefer (1991). Only material from the upper trap was used for comparison with data from the ParCa system at 995 m and the INFLUX system at 1015 m water depth.

3. Results and discussion

a. Particle abundance profiles. Six vertical profiles through the upper 550 m of the water column were completed during R.V. *Meteor* M22-1 and M23-3 in fall 1992 and

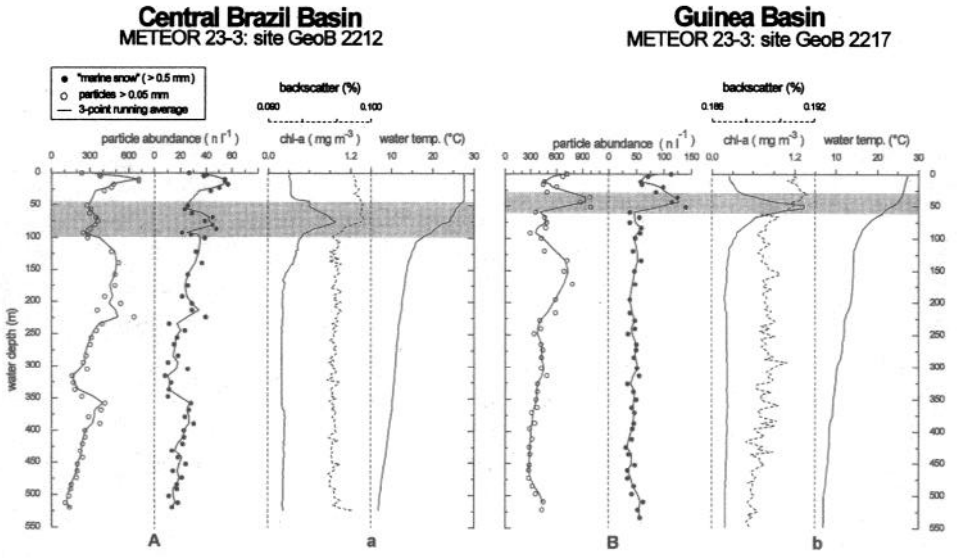

Figure 3. Vertical particle abundance profiles (A, B) and INFLUX derived data of optical backscatter, chlorophyll-*a* and water temperature (a, b) observed at two stations (site GeoB 2212: 04°00.4′S; 25°37.1′W; site GeoB 2217: 00°00.5′N, 10°49.8′W) in the equatorial Atlantic Ocean during R. V. *Meteor* cruise M 23-3 in March 1993.

spring 1993 on oceanographic sampling sites and mooring stations in the equatorial Atlantic Ocean and off the West African shelf. Here we describe two of these particle abundance profiles obtained with the ParCa system on cruise M23-3 at sampling sites GeoB 2212 (04°00.4′S; 25°37.1′W) and GeoB 2217 (00°00.5′N; 10°49.8′W) aboard R.V. *Meteor* in the equatorial Atlantic Ocean, both completed in March 1993 (Fig. 3). Site GeoB 2212 was located in the central Brazil Basin, whereas site GeoB 2217 was situated within the equatorial Guinea Basin. The profiles show variable distributions of particles and aggregates between the ocean's surface and 550 m water depth, with major concentrations occurring in the upper 80 meters. Though a significant part of the photographed particles belongs to the size class of marine snow, typical flocs and fractal shaped aggregates reported elsewhere (Syvitsky *et al.,* 1995; Lampitt, 1985; Logan and Wilkinson, 1990) were not found during either profile. Both images and INFLUX-derived data of fluorescence (chlorophyll-*a*) and optical backscatter show a shift of the chlorophyll-*a* maximum corresponding to the upward shift of the thermocline from a water depth of 75 m in the west (site GeoB 2212, Fig. 3a) to 50 m in the east (site GeoB 2217, Fig. 3b). Total number of particles reached from 125 (512 m) to 677 (10 m) counts per liter in the oligotrophic Brazil Basin (Fig. 3A), and from 281 (461 m) to 991 (36 m) in the equatorial upwelling area of the Guinea Basin (Fig. 3B). Particles and aggregates in the size class of marine snow (>0.5 mm) show abundances of 8 to 57 and 34 to 127 counts per liter, with distinctive peaks observed at the thermocline-base, corresponding to the chloro-

phyll-*a* maximum observed with the INFLUX-current meter. In contrast, both profiles show distinctive particle abundance maxima below 100 m depth, which are not represented in the INFLUX measurements of backscatter, chlorophyll-*a* and water temperature. While two peaks in the central Brazil Basin at 220 and 305 m seem to consist of the entire measured particle size spectrum, the broad maximum around 150 m depth in the Guinea Basin is not reflected by the marine snow abundance. These peaks are not seen in backscattering at either site.

b. Particle abundances and concentrations during long-term deployment. For instrument testing and data acquisition, ParCa was deployed at 995 m water depth in Summer 1994 on the sediment-trap mooring CI4 located in the Canary Basin (29°09.1'N; 15°26.5'W). After three month of deployment between June and September, the system was recovered. During this time, at alternating 7.5 and 15 hour intervals one double-exposed frame was exposed.

Figure 4 shows the results of the ParCa deployment (Fig. 4A, B) in comparison to the optical INFLUX data (Fig. 4C) from 1015 m depth. Figure 5 shows the total flux record of the simultaneously deployed upper sediment trap (Fig. 5A) at 923 m, and over sampling-time of 4.3 days integrated particle volumes of the ParCa-derived data from 995 m water depth (Fig. 5B, C). Current speeds at 1015 m depth in the area below camera and trap show both a high (dicl) and low frequent variation but never exceeded 10 cm s^{-1} (Fig. 5D). Thus, we assume that hydrodynamic biases at the trapping site were minimal (Baker *et al.,* 1988; Gust *et al.,* 1992).

Two major events occur in the total flux record derived from the sediment trap at 925 m depth (Fig. 5A). The first broad maximum in the second half of June contains the highest flux of particulate matter with 67.2 mg m^{-2} d^{-1}. A second, much smaller event was recorded with a total flux of 26.9 mg m^{-2} d^{-1} between July 17th and 21st in sample 10. Sample 15 contains fish-parts and swimmers and was therefore excluded from further calculations. The lowest total particle flux during deployment time was recorded in sample 19 with 2.8 mg m^{-2} d^{-1}. In comparison, the ParCa-derived distribution of particles >0.05 mm shows a more differentiated abundance pattern with high temporal variations of 47 to 164 particles per liter during the first 50 days of deployment. This is mainly driven by particles <0.5 mm with abundances between 38 and 151 counts l^{-1} (Fig. 4A). In contrast, particles >0.5 mm account for most of the calculated volume distribution, as shown in (Fig. 4B). Highest particle volumes of up to 6.48 mm^3 l^{-1} occur within the first flux event during the second half of June. In mid-July, the second flux maximum is represented by values of up to 5.6 mm^3 l^{-1} between the 13th and 17th of July. Figure 5B and 5C show volume data of marine snow sized particles, integrated over 4.3 days, while Figure 5C gives the results of the data corrected by a three-day offset in the start time of the camera. Due to a readout failure it is likely that a certain start time offset took place, but unfortunately there is no way to quantify this precisely. A delay greater than three days is not possible

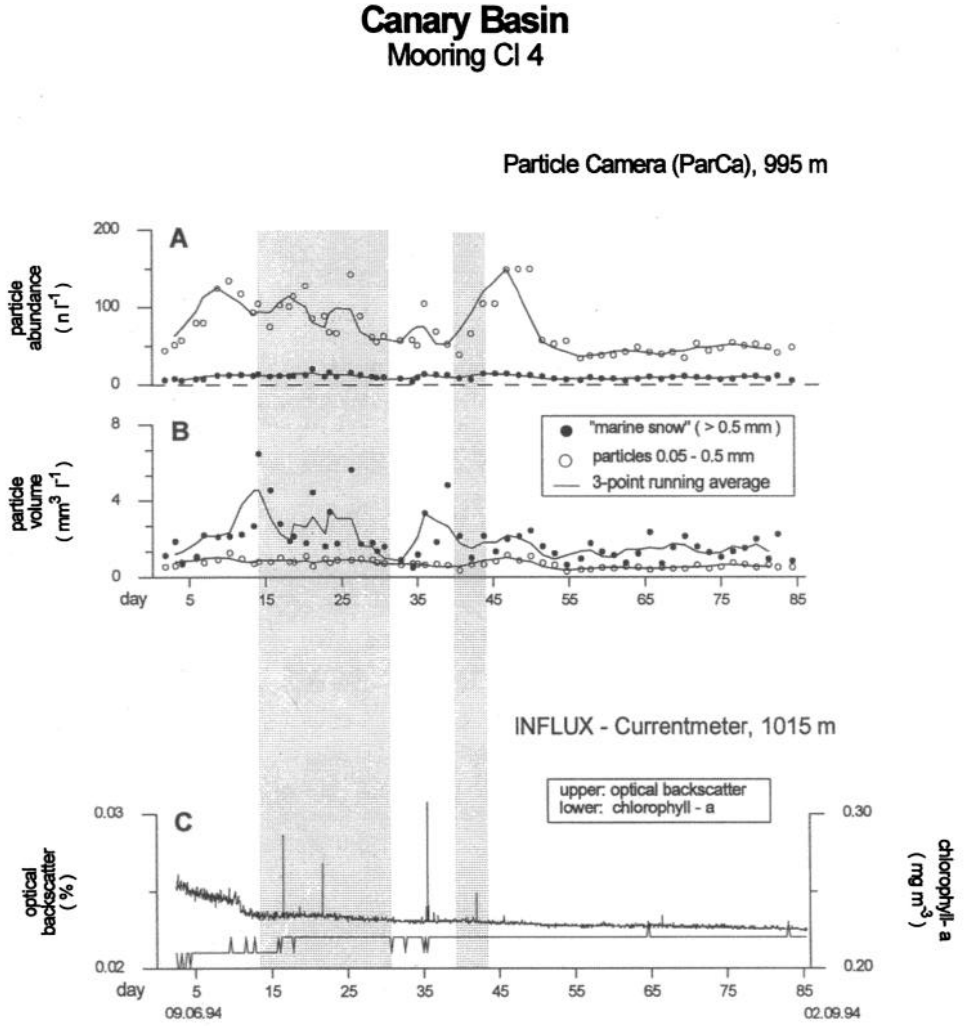

Figure 4. Results of the ParCa system (A, B) and the optical sensors of the simultaneously deployed INFLUX currentmeter (C) at mooring-station CI 4 (29°09.1'N; 15°C26.5'W) in the Canary Basin, between June and September 1994. Gray areas refer to sediment trap derived peaks in total particle flux as shown in Figure 5.

because the program of 420 exposures was correctly finished when the system was recovered on 4 September, 1994. Both figures show the similar trends compared to the flux record of the sediment trap; but, in detail, the data corrected by the three-day offset provide the better fit (Fig 6B). This result supports previous findings that relatively rare aggregates and large particles contribute to most of the particle flux recorded with sediment traps (e.g. Deuser *et al.,* 1981; Asper, 1987; Gardner and Walsh, 1990; Walsh and Gardner, 1992).

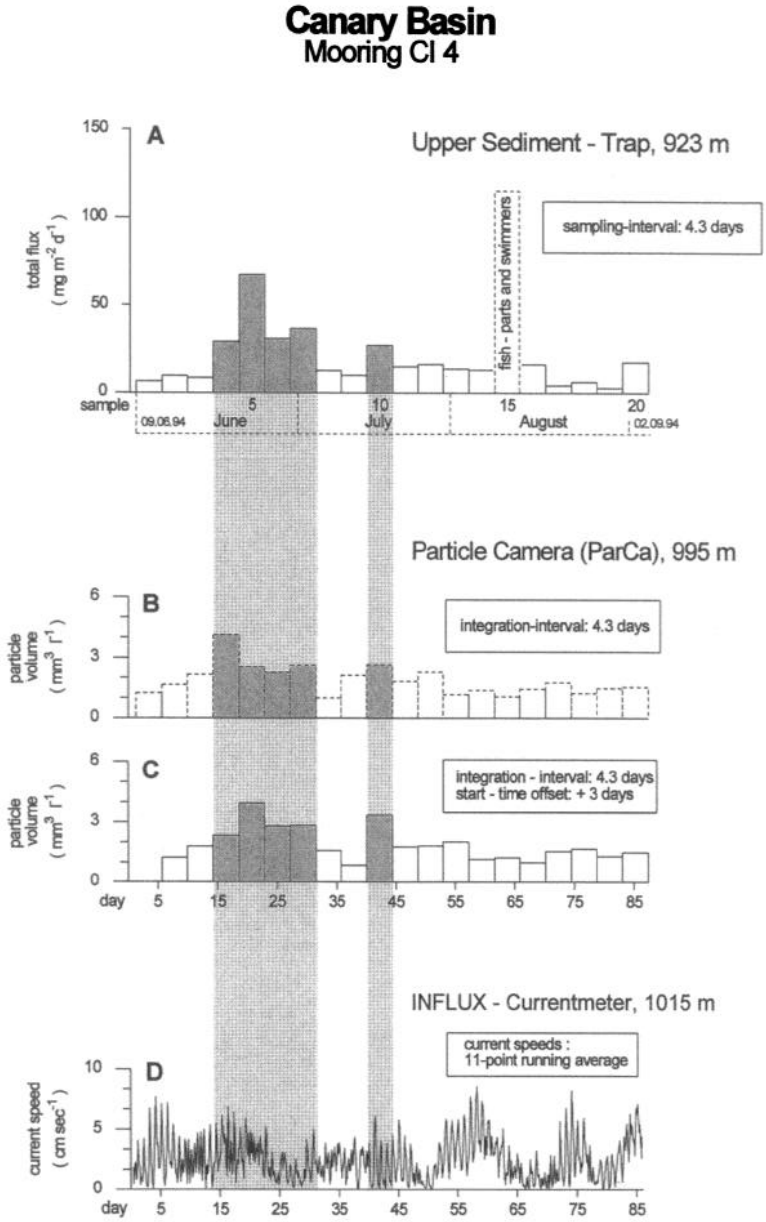

Figure 5. Sediment trap derived total particle fluxes (A), integrated particle volumes calculated from ParCa images (B, C) and currentspeeds recorded with the INFLUX current-meter (D) at mooring-station CI 4 (29°09.1'N; 15°26.5'W) in the Canary Basin, between June and September 1994.

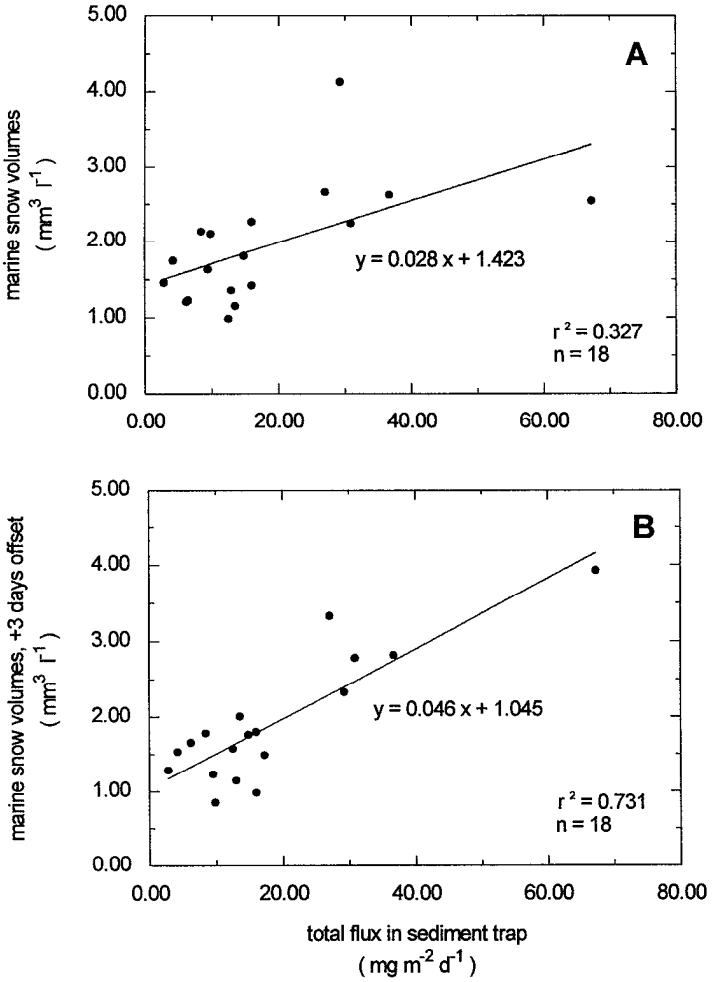

Figure 6. Correlations of ParCa-derived marine snow volume concentration and total particle flux recorded with the upper sediment trap at station CI 4 in the Canary Basin. (A) shows "raw" particle volumes as plotted in Fig. 5B versus total particle flux, (B) gives the result of adding a 3-day offset to particle volume data (see text) as plotted in Figure 5C.

In contrast to the two depth profiles described before, optical backscatter and chlorophyll-*a* concentration do not follow any of the trends of the total particle abundance (Fig. 4C), and both show significantly lower values. Very low backscatter values around 0.05% have previously been reported at this site between July and September in almost the same water depth (900 m) by Fischer *et al.* (1996) between sedimentation events. This may be partly due to the much lower abundance of particles during the deployment at 1000 m depth compared to the other data obtained in the upper 600 m of the water column. Furthermore, the deployment time

is known to be a low production period. During spring, much higher total fluxes of up to 128 mg m^{-2} d^{-1} are reported from previous studies at the same site, where short-term sedimentation pulses could be recorded with sediment traps as well as with the chlorophyll-*a* sensor of the INFLUX currentmeter (Fischer *et al.,* 1996). However, during the ParCa deployment single peaks in the optical backscatter occur only during or in between the two described particle flux events, whereas chlorophyll does not show any significant variance.

In addition to previous work with sediment trap moorings the study described in this paper offers for the first time a direct comparison of sediment trap derived flux measurements with optical data of chlorophyll-*a*, Mie-backscatter and *in-situ* accessed images of marine particles. This approach provides more information on *in-situ* particle dynamics and composition of sinking material and may lead to a more detailed understanding of mass fluxes in open ocean conditions.

The results described here indicate that none of the observation methods used during the profiles or moored deployment shows the entire particle community: while the camera system does not resolve the distribution of smallest particles contributing to the backscatter signal of the currentmeter, the INFLUX sensors do not reflect changes in the distribution of particles greater than 0.05 mm. On the other hand, the simultaneous use of both systems in addition to sediment traps provides information on the different behavior of different size classes of marine particles, indicating that the smaller size classes of marine particles show less variance through depth and time than large aggregates and marine snow (Gardner and Walsh, 1990; Lampitt *et al.,* 1993; Syvitski *et al.,* 1995). This is of particular interest for abundance and mass esimates of slowly versus rapidly sinking particulate matter (Alldredge and Silver, 1988; Gardner and Walsh, 1990; Syvitski *et al.,* 1995). The comparable trends in particle abundance, marine snow volume concentrations and total particle fluxes reported here allow a use of this dataset for further computation of *in situ* measured particle distributions versus particle fluxes and sinking speeds, which will be presented in a following paper.

Acknowledgments. We thank the masters and the crews of the research vessels FS *Polarstern* and FS *Meteor* for the their professional help during deployment and recovery of the ParCa system and the mooring array. Special thanks are due to G. Fischer for many hours of creative discussion, careful reading of the manuscript and making helpful suggestions, and to G. Ruhland for innumerable comments and help during development of the ParCa system. We are also grateful to G. Krause for providing the INFLUX systems used during profiles and deployment, and to P. Gerchow, R. Heygen, U. Rosiak, R. Plugge and H. Pabst for technical assistance at sea. Laboratory work performed by V. Diekamp and C. Slickers is gratefully acknowledged. We would also like to thank the two anonymous referees for their comments which improved the paper. This research was funded by the Deutsche Forschungsgemeinschaft (Sonderforschungsbereich 261 at Bremen University, Contribution 113).

REFERENCES

Alldredge, A. L. and M. W. Silver. 1988. Characteristics, dynamics and significance of marine snow. Prog. Oceanogr. *20,* 41–82.

Asper, V. L. 1987. Measuring the flux and sinking speed of marine snow aggregates. Deep-Sea Res., *34,* 1–17.

Asper, V. L., S. Honjo and T. H. Orsi. 1992. Distribution and transport of marine snow aggregates in the Panama Basin. Deep-Sea Res., *39,* 939–952.

Baker, E. T., H. B. Milburn and D. A. Tennant. 1988. Field assumption of sediment trap efficiency under varying flow conditions. J. Mar. Res., *46,* 573–592.

Costello, D. K., K. L. Carder, P. R. Betzer and R. W. Young. 1989. *In situ* holographic imaging of settling particles: Applications for individual particle dynamics and oceanic flux measurements. Deep-Sea Res., *36,* 1595–1605.

Deuser, W. G. 1986. Seasonal and interannual variations in the deep-water particle fluxes in the Sargasso Sea and their relation to surface water hydrography. Deep-Sea Res., *33,* 225–246.

Deuser, W. G., E. H. Ross and R. F. Anderson. 1981. Seasonality in the supply of sediment to the deep Sargosso Sea and implications for the rapid transport of matter to the deep ocean. Deep-Sea Res., *28,* 495–505.

Fischer, G., G. Krause, S. Neuer and G. Wefer. 1996. Short-term sedimentation pulses recorded with a chlorophyll sensor and sediment traps in 900 m water depth in the Canary Basin. Limnol. Oceanogr., (submitted).

Fischer, G. and G. Wefer. 1991. Sampling, preparation and analysis of marine particulate matter, *in* The Analysis and Characterization of Marine Particles, D. C. Hurd and W. Spencer eds., AGU, Washington, 391–397.

Gardner, W. D. and M. J. Richardson. 1992. Particle export and resuspension fluxes in the western North Atlantic, *in* Deep-Sea Food Chains and the Global Carbon Cycle, G. T. Rowe and V. Pariente, ed., Kluwer Academic Publishers, 339–364

Gardner, W. D. and I. D. Walsh. 1990. Distribution of macroaggregates and fine-grained particles across a continental margin and their potential role in fluxes. Deep-Sea Res., *37,* 401–411.

Gorsky, G., C. Aldorf, M. Kage, M. Picheral, Y. Garcia and J. Favole. 1992. Vertical distribution of suspended aggregates determined by a new underwater video profiler. Ann. Inst. Oceanogr., *68,* 275–280.

Gust, G. R., R. H. Byrne, R. E. Bernstein, P. R. Betzer and W. Bowles. 1992. Particle fluxes and moving fluids: experience from synchronous trap collections in the Sargasso Sea. Deep-Sea Res., *39,* 1071–1083.

Hecker, B. 1990. Photographic evidence for the rapid flux of particles to the sea floor and their transport down the continental slope. Deep-Sea Res., *37,* 1773–1782.

Heffler, D .E., J. P. M. Syvitski and K. W. Asprey. 1991. The floc camera, *in* Principles, Methods and Application of Particle Size Analysis, J. P. M. Syvitski, ed., Cambridge University Press, New York, 209–221.

Honjo, S., K. W. Doherty, Y. C. Agrawal and V. L. Asper. 1984. Direct optical assessment of large amorphous aggregates (marine snow) in the deep ocean. Deep-Sea Res., *31,* 67–76.

Honjo, S., S. Manganini and J. J. Cole. 1982. Sedimentation of biogenic matter in the deep ocean. Deep-Sea Res., *29,* 609–625.

Kajihara M. 1971. Settling velocity and porosity of large suspended particles. J. Oceanogr. Soc. Japan, *27,* 158–162.

Krause, G. and K. Ohm. 1996. The INFLUX current meter and its use together with a sediment trap. Deep-Sea Res., (submitted).

Lampitt, R. S. 1985. Evidence for the seasaonl deposition of detritus to the deep-sea floor and its subsequent resuspension. Deep-Sea Res., *32,* 885–897.

Lampitt, R. S., W. R. Hillier and P. G. Challenor. 1993. Seasonal and diel variation in the open ocean concentration of marine snow aggregates. Nature, *362,* 737–739.

Logan, B. E. and D. B. Wilkinson. 1990. Fractal geometry of marine snow and other biological aggregates. Limnol. Oceanogr., *35,* 130–136.

MacIntire, S., A. L. Alldredge and C. C. Gotschalk. 1995. Accumulation of marine snow at density discontinuities in the water column. Limnol. Oceanogr., *40,* 449–468.

McCave, I. N. 1975. Vertical flux of particles in the ocean. Deep-Sea Res., *22,* 491–502.

Shanks, A. L. and J. D. Trent. 1980. Marine now: Sinking rates and potential role in vertical flux. Deep-Sea Res., *27A,* 137–143.

Silver, M. W. and A. L. Alldredge. 1981. Bathypelagic marine snow: deep-sea algal and detrital community. J. Mar. Res., *39,* 501–530.

Syvitski, J. P., K. W. Asprey and K. W. G. Leblanc. 1995. *In-situ* characteristics of particles settling within a deep-water estuary. Deep-Sea Res. II, *42,* 223–256.

Walsh, I. D. and W. D. Gardner. 1992. A comparison of aggregate profiles with sediment trap fluxes. Deep-Sea Res., *39,* 1817–1834.

Wefer, G. 1989. Particle flux in the ocean: Effects of episodic production, *in* Productivity of the Oceans: Present and Past. W. H. Berger, V. S. Smetacek and G. Wefer, eds., Wiley and Sons, 139–153

Received : *15 August, 1995;* revised; *14 November, 1995.*